







# A Wideband RF Power Divider With Ultra-Wide Harmonics Suppression

SIKANDAR ABBAS <sup>1</sup> (Student Member, IEEE), MOAZAM MAQSOOD <sup>2</sup> (Member, IEEE),  
NOSHERWAN SHOAIB <sup>3</sup> (Senior Member, IEEE),  
MUHAMMAD QASIM MEHMOOD <sup>1</sup> (Senior Member, IEEE),  
MUHAMMAD ZUBAIR <sup>4</sup> (Senior Member, IEEE), AND YEHIA MASSOUD <sup>4</sup> (Fellow, IEEE)  
(Regular Paper)

<sup>1</sup>MicroNano Lab, Department of Electrical Engineering, Information Technology University of the Punjab, Lahore 56000, Pakistan

<sup>2</sup>Pak-Austria Fachhochschule: Institute of Applied Sciences and Technology, Mang Haripur 22620, Khyber Pakhtunkhwa, Pakistan

<sup>3</sup>School of Electrical Engineering & Computer Sciences (SECS), National University of Sciences and Technology (NUST), Islamabad 44000, Pakistan

<sup>4</sup>Innovative Technologies Laboratories (ITL), King Abdullah University of Science and Technology (KAUST), Thuwal 23955-6900, Saudi Arabia

CORRESPONDING AUTHORS: Muhammad Qasim Mehmood, Muhammad Zubair, Yehia Massoud (e-mails: qasim.mehmood@itu.edu.pk, muhammad.zubair.3@kaust.edu.sa, yehia.massoud@kaust.edu.sa).

This work was supported in part by the Innovative Technologies Laboratories—KAUST, and in part by the PHEC PIRCA Award.

**ABSTRACT** This article reports a wide-band power divider with ultra-wide harmonic suppression. The filtering power divider consists of a Wilkinson power divider and a filter merged into a single structure. For filtering purposes, a novel suppressor cell is designed using resonators of various shapes. The power divider exhibits an operational frequency of 1.64 GHz, encompassing a fractional bandwidth (FBW) of 57 percent, ranging from 1.151 GHz to 2.08 GHz. Notably, it effectively suppresses a total of 24 harmonics, attaining a rejection level exceeding  $-15$  dB. The measured in-band isolation, input return loss, insertion loss, and output return loss are determined at 1.64 GHz to be  $-23$  dB,  $-36$  dB,  $-3.03$  dB, and  $-18$  dB, respectively. These results showcase the superior performance of the proposed design compared to existing state-of-the-art solutions.

**INDEX TERMS** Harmonic suppression, power divider, low pass filter, wide operating band, ultrawide stopband.

## I. INTRODUCTION

Power dividers are one of the basic elements of a wireless communication system. Common power dividers used in RF systems are T-junction, resistor-based, and Wilkinson [1] power dividers with the latter being the most popular one. [2]. Equal power division with lossless matching at all ports along with isolation at coupling ports are a few advantages of the Wilkinson power divider over the other available options. Antenna arrays, mixers, amplifiers (Doherty, Low Noise), and phase shifters are common components of a communications chain for transmission and reception. An inherent disadvantage these devices suffer from is the harmonics created due to the non-linearity of the active components. This reduces system linearity and produces intermodulation products. The Wilkinson power divider, although a popular component, permits the passage of these harmonics. To reject the unwanted

harmonics in power dividers, the filtering capability is incorporated within the power divider circuit by creating different modifications to the filter design. Various techniques have been proposed in the literature for this purpose. These include open stubs, coupled lines, electromagnetic bandgap (EBG), defective ground structures (DGS), patch resonators, and LC components. The aforementioned techniques and design details are presented in the following section. The suppression of harmonics using open and short-circuited stubs is described in [3], [4], [5]. The proposed techniques have the benefit of having a simple structure. Each individual stub is only capable of suppressing a single harmonic. As a result, many stubs are required for ultra-wide suppression, which can make the circuit complex and large. Harmonic suppression in power dividers by using coupled lines is presented in [6], [7], [8], [9], [10]. Coupled lines have the advantage of achieving a

wider stopband along with a wider operating band. However, insertion loss within the operating band is also higher.

Harmonics suppression by using a defective ground structure is achieved in [11]. The technique is advantageous in that it provides a wider stopband but requires an additional etching process for fabrication. Back radiation is another disadvantage of a defective ground structure (DGS) which can affect other microwave components. Electromagnetic bandgap (EBG) is also proposed for harmonic suppression in [12]. The presented designs produce satisfactory results, providing effective suppression. Like DGS, EBG also requires additional fabrication steps, making the overall design more complex. In [13], a power divider using double-sided parallel transmission lines is presented. Changing the bowtie cell parameters can alter the operating frequency. Although the proposed design has an ultra-wide stopband, it has a complex circuit. A high-isolation filtering power divider with harmonic suppression is described in [14]. To accomplish superior isolation performance, this power divider employs complex impedance rather than a pure resistor. Notably, the design effectively eliminates six harmonics, substantially enhancing the device's overall filtering capabilities. Lumped components in conjunction with transmission lines are proposed in [15] as a hybrid technique for harmonic suppression. The presented design is very compact and easy to create, but it has limited bandwidth. Harmonic suppression by integrating power dividers with resonators has been presented in [16], [17], [18], [19], [20], [21], [22], [23]. Proposed designs use resonators such as patches, rings, triangular, and defect-shaped resonators, which are simple in design, but passband and stopband require attention.

This research article presents the design of a wide-band power divider with an ultra-wide stopband. The proposed design incorporates a novel resonating structure, referred to as a suppressor cell, into a standard Wilkinson power divider. The suppressor cell is created by combining two oval-shaped resonators, one rectangular-shaped resonator, one radial-shaped resonator, and one open stub. The designed suppressor cell has a broad operating spectrum and effectively suppresses harmonics up to 40 GHz. The power divider, designed for operation at 1.64 GHz, demonstrates the ability to suppress harmonics over a broad frequency range. The results of the suggested design are compared with those of the most recent power dividers, and it is demonstrated that the proposed design achieves better performance in comparison to the previous research. The key contribution of this work includes a wide operating band, ultrawide harmonics suppression, compact size, and straightforward design. In contrast to the recent work that has been proposed, the design work possesses high performance on the planar structure.

## II. POWER DIVIDER CIRCUIT DESIGN

This section explains the circuit design of the proposed power divider. As explained earlier, harmonic suppression is achieved by replacing the transmission lines of the Wilkinson power divider with a resonating suppressor cell. Two oval-shaped resonators, one rectangular-shaped resonator,

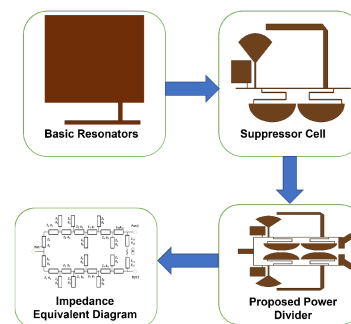


**FIGURE 1.** Design flow of the proposed power divider.

one radial-shaped resonator, and one open stub are used to construct the suppressor cell. Two of these components are separately integrated with the transmission lines of the Wilkinson divider. Fig. 1 shows the design flow. The entire design process is detailed below. A commercial EM solver Advanced Design System (ADS) is utilized for simulation, and EM simulations are performed. Rogers 5880 substrate with a thickness of 0.787 millimeters is used.

### A. RECTANGULAR SHAPE RESONATOR

Fig. 2(a) illustrates a rectangular-shaped resonator, which exhibits a cut-off frequency of 10 GHz, as depicted in Fig. 2(b). The resonator effectively provides a rejection band spanning from 11.77 GHz to 40 GHz, characterized by an attenuation level of  $-14$  dB. Notably, within the frequency range of 11.80 GHz to 15 GHz, the resonator demonstrates significant attenuation of  $-15$  dB, thus offering a bandwidth of 3.2 GHz. Additionally, the dominant mode of the resonator manifests as a transmission zero at 13.12 GHz, exhibiting a rejection level of  $-37$  dB. This can be observed in Fig. 2(c), where the current distribution at 13.12 GHz illustrates a complete absence of current flow from port 1 to port 2.

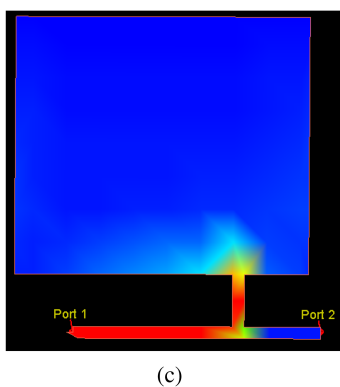
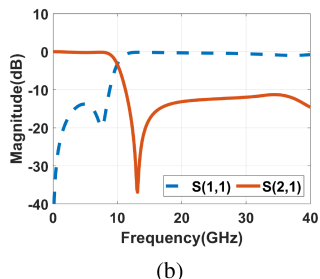
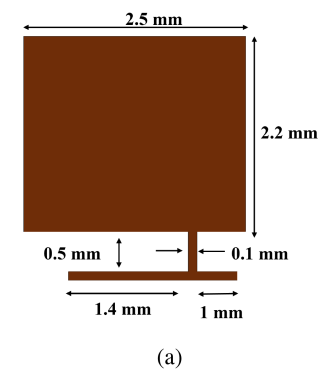
### B. RADIAL SHAPE RESONATOR

Fig 1(a) shows a radial-shaped resonator. The resonator response is presented in 3(a) showing a cut-off frequency at 5.72 GHz and transmission zero ( $-35.013$  dB) at 6.56 GHz. The frequency response analysis of radial-shaped resonators reveals a suppression bandwidth spanning a width of 1 GHz.

It can be seen in Fig. 3(b) the radial-shaped resonator has only one resonance thereby being the dominant mode. Fig. 3(c) presents the current distribution of the resonator and it can be seen that at 6.56 GHz no current is flowing from port 1 to port 2.

### C. SUPPRESSOR CELL ONE

By integrating both radial and square-shaped resonators, substantial enhancements have been achieved in the overall system performance. The layout and frequency response are shown in Fig. 4(a) and (b) receptivity. The combination of these resonator types has synergistically contributed to enhanced sharpness and increased bandwidth, expanding from



**FIGURE 2.** (a) Layout diagram of rectangular shape resonator (simulated) (b) Frequency response of rectangular shape resonator (c) Current distribution at 13.12 GHz of the rectangular-shaped resonator (simulated).

3 GHz to 8 GHz with a significant attenuation of  $-15$  dB. Despite these advancements, further refinements are required to achieve optimal wideband suppression.

**D. OVAL SHAPE RESONATOR**

Fig. 5(a) showcases the layout of an oval-shaped resonator, while Fig. 5(b) presents its corresponding frequency response. This resonator exhibits three distinct resonances at frequencies of 3.53 GHz, 14.33 GHz, and 29 GHz, accompanied by attenuation levels of  $-36$  dB,  $-30$  dB, and  $-20$  dB, respectively. Each resonance is characterized by its specific bandwidth, which delineates the frequency range in which it operates. The first resonance demonstrates a bandwidth of 750 MHz, spanning from 3.32 to 4.07 GHz. The second resonance boasts a broader bandwidth of 2.2 GHz, extending from 13.71 to 15.91 GHz. Notably, the third resonance showcases an even wider bandwidth of 3.69 GHz, spanning from 28 to

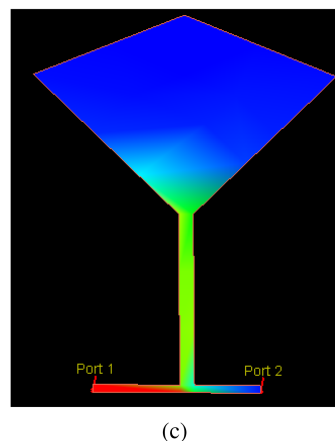
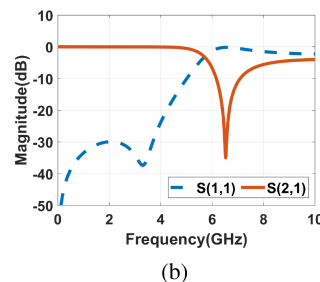
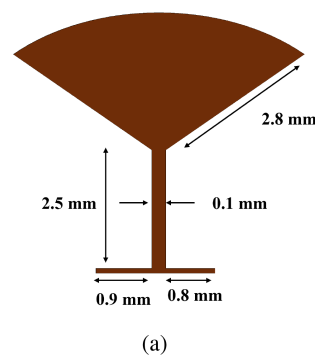


**FIGURE 3.** (a) Layout diagram of radial shape resonator (simulated) (b) Frequency response of radial shape resonator (c) Current distribution at 6.56 GHz of the radial-shaped resonator (simulated).

31.691 GHz. The presence of these resonances signifies the resonator’s ability to operate across an expanded frequency band, rendering it suitable for higher frequency applications. In Fig. 5(c)–(e), it is observed that there is no current flow between ports 1 and 2 at the frequencies corresponding to these resonances. Among the three resonances, the dominant mode is observed at 29 GHz within the oval-shaped resonator.

**E. SUPPRESSOR CELL TWO**

By implementing a cascaded configuration of oval-shaped resonators in conjunction with the main resonator, significant improvements have been observed compared to the previous design. The suppressor cell’s layout can be visualized in Fig. 6(a), while the frequency response of the system to different frequencies is depicted in Fig. 6(b). Notably, two prominent bandwidths of unwanted frequency suppression

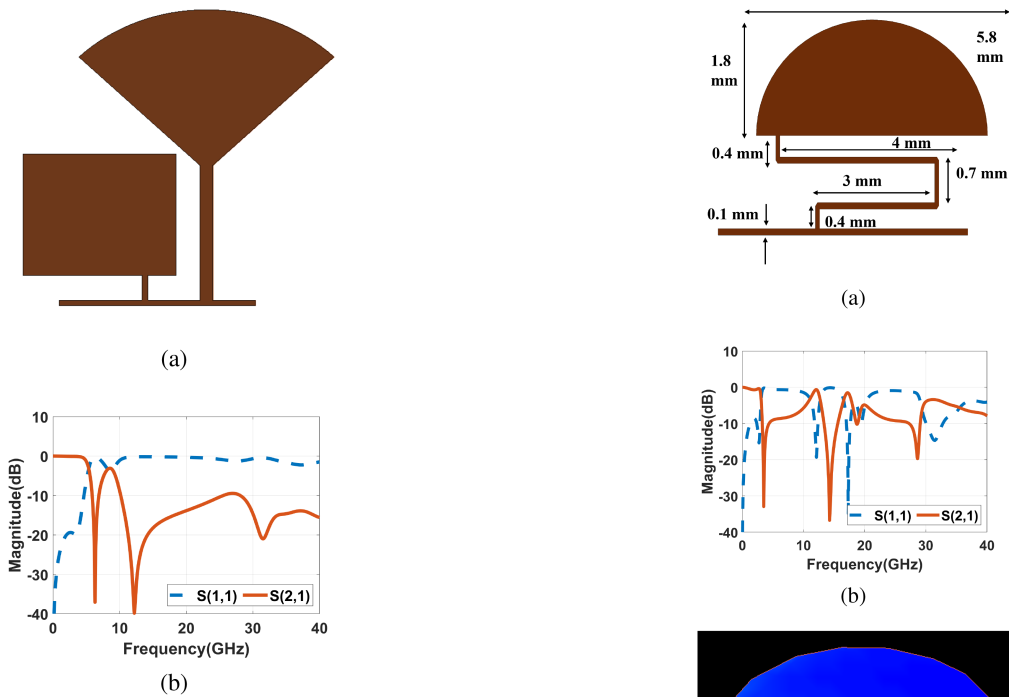


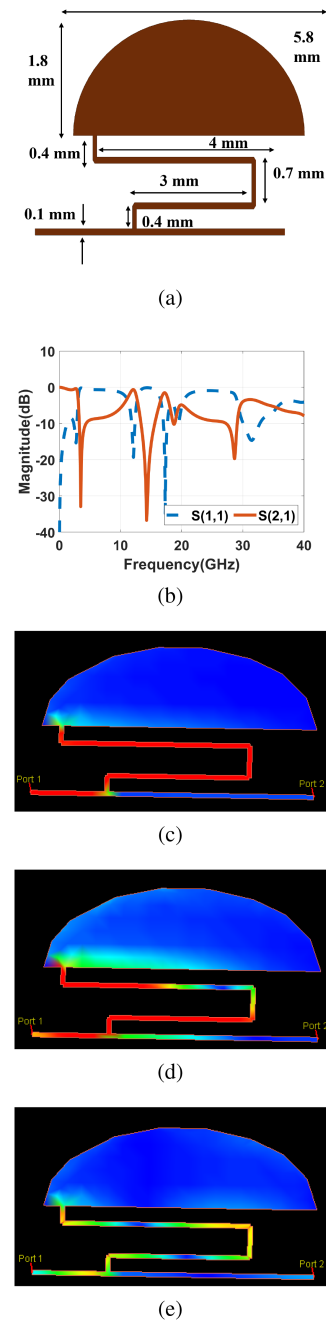
**FIGURE 4.** (a) Layout diagram of suppressor cell one (simulated) (b) Frequency response of suppressor cell one.

have been achieved. The first bandwidth spans from 5.27 to 17.08 GHz, providing a width of 13 GHz for effective suppression. The second bandwidth ranges from 25.74 GHz to 40 GHz, with a width of 12.28 GHz. Despite these advancements, further enhancements are still required to achieve sharper suppression characteristics.

A further improvement has been made to the previous resonator design, as shown in Fig. 7(a). An additional oval-shaped resonator has been added to the existing suppressor cell. This modification has resulted in better performance, which is demonstrated by the frequency response shown in Fig. 7(b). With the addition of the extra resonator, three main frequency bands with strong attenuation have been achieved. The first band spans from 3 GHz to 8 GHz, covering a width of 5 GHz. The second band ranges from 10.62 GHz to 22.71 GHz, which is a width of 24 GHz. Lastly, there is a band from 24 GHz to 40 GHz with high attenuation. Despite the overall improvements in the resonator design, there are still specific frequency ranges where the suppression performance could be enhanced. Particularly, between 8 GHz and 10.60 GHz, and between 20 GHz and 25 GHz, the suppression of unwanted frequencies is not as effective. In these ranges, the attenuation levels are below  $-10$  dB, indicating that further improvements are needed to achieve the desired level of suppression.

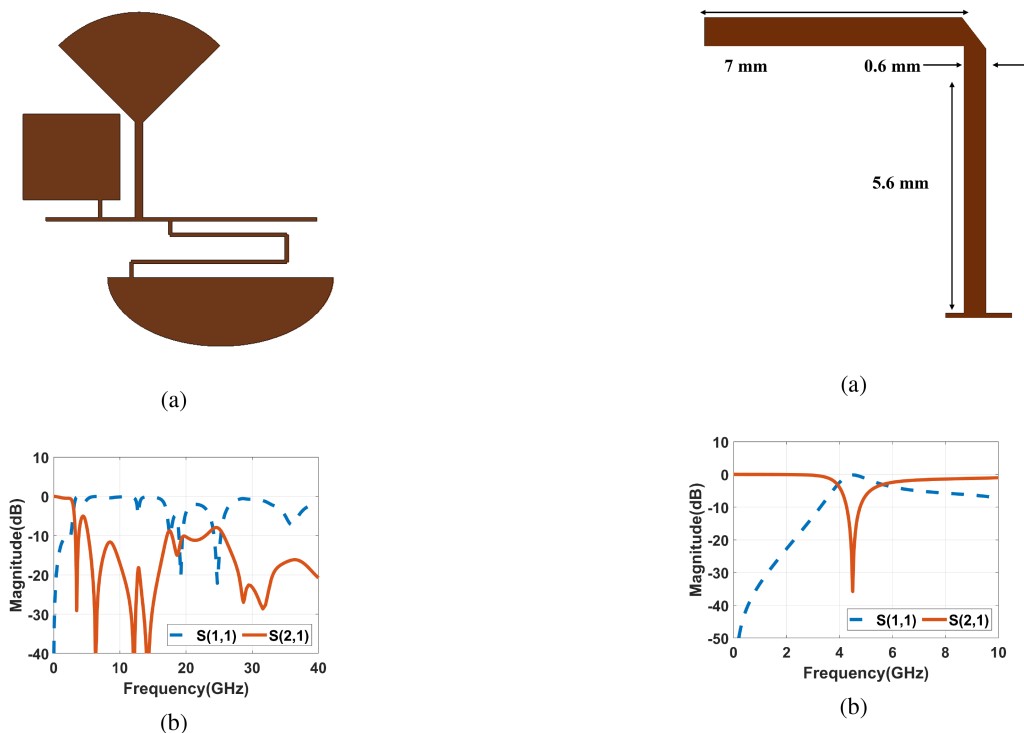
#### F. OPEN STUB RESONATOR

Fig. 8(a) illustrates an open stub, which serves as a suppressor cell. This open stub design results in a transmission zero occurring at 4.5 GHz, accompanied by an attenuation level



**FIGURE 5.** (a) Layout diagram of oval shape resonator (simulated) (b) Frequency response of oval shape resonator (c) Current distribution at 3.53 GHz of the oval-shaped resonator (simulated) (d) Current distribution at 14.33 GHz of the oval-shaped resonator (simulated) (e) Current distribution at 29 GHz of the oval-shaped resonator (simulated).

of  $-35.78$  dB, as presented in Fig. 8(b). Upon analyzing the frequency response, it is observed that the open stub resonator provides a suppression bandwidth of 1 GHz. Additionally, Fig. 8(c) depicts the current distribution within the open stub structure. The open stub exhibits a single resonance at 4.5 GHz, making it the dominant mode of the resonator at this frequency. At this resonant frequency, no current flows from port 1 to port 2.



**FIGURE 6.** (a) Layout diagram of suppressor cell two part 1 (simulated) (b) Frequency response of suppressor cell two part 1.

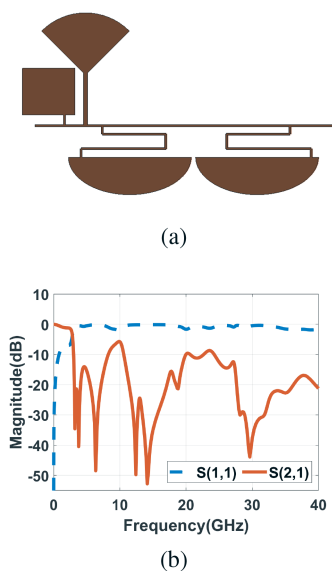


**FIGURE 7.** (a) Layout diagram of suppressor cell two part 2 (simulated) (b) Frequency response of suppressor cell two part 2.

**G. PROPOSED SUPPRESSOR CELL**

A suppressor cell is designed by combining all the above resonators and stubs, as shown in Fig. 9(a). Two oval-shaped resonators, one rectangular-shaped resonator, one radial-shaped resonator, and one open stub. In Fig. 9(b) the equivalent impedance diagram is shown. Simulation results of the combined structure are shown in Fig. 9(c) where an extremely

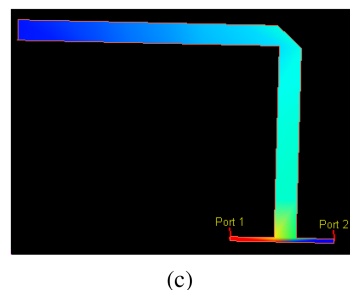


**FIGURE 8.** (a) Layout diagram of open stub resonator (simulated) (b) Frequency response of open stub resonator (c) Current distribution at 4.5 GHz of the open stub resonator (simulated).

broad stopband can be seen. As shown in Fig. 9(c), the suppressor cell has a cut-off frequency of 2.75 GHz.

**H. PROPOSED POWER DIVIDER**

Fig. 10(a) showcases the complete design layout of the proposed power divider. The frequency response of the power divider within its operating band is presented in Fig. 10(b) and Fig. (c), while Fig. 10(d) provides a comprehensive overview of its frequency response.

In Fig. 10(b), the return loss and insertion loss characteristics of the power divider within the operating band are depicted, and Fig. 10(c) highlights the isolation and output return loss characteristics within the same frequency range. The power divider exhibits a frequency range spanning from 1.151 GHz to 2.083 GHz, corresponding to a 57% fractional bandwidth with a -15 dB attenuation level. Its central frequency is precisely set at 1.64 GHz. Notably, the power divider showcases exceptional performance in the form of an ultra-wide stopband, effectively rejecting signals at a level of

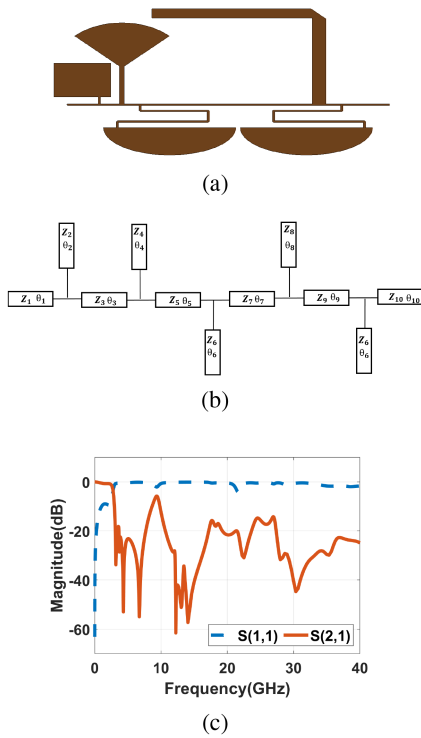


**FIGURE 9.** (a) Layout diagram of suppressor cell (simulated) (b) Equivalent impedance diagram of suppressor cell (c) Frequency response of suppressor cell.

–15 dB up to 40 GHz. Consequently, it successfully suppresses harmonics ranging from the 2nd to the 24th across the entire stopband.

The passband of the power divider, as represented by S11, S21, S22, and S23, exhibits the following dB values at 1.64 GHz: –36 for return loss, 3.03 for insertion loss, –23 for isolation, and –18 for output return loss.

Fig. 10(d) provides a comprehensive representation of the power divider’s overall frequency response, encapsulating its various characteristics and performance metrics within the designated operating band.

### I. THEORETICAL DESIGN

The numerical evaluation of the S-parameters of the proposed power divider (return loss and insertion loss) is calculated using Even-Odd mode method. To evaluate the theoretical design, equivalent circuits of the complete power divider and the relative Even-Odd modes have been presented in Fig. 11(a)–(c). Fig. 11(b) is used for the calculation of return loss while 11(c) is used for the insertion loss. For calculating the input reflection coefficient, excitation from the left is assumed. Equation (1) gives the reflection coefficient,  $S_{11}$  [1].

$$S_{11} = \Gamma_{in}^e = \frac{Z_A - 2Z_0}{Z_A + 2Z_0} \quad (1)$$

The return loss that is calculated from (1) is given below.

$$RL(dB) = -20 \cdot \log |S_{11}| \quad (2)$$

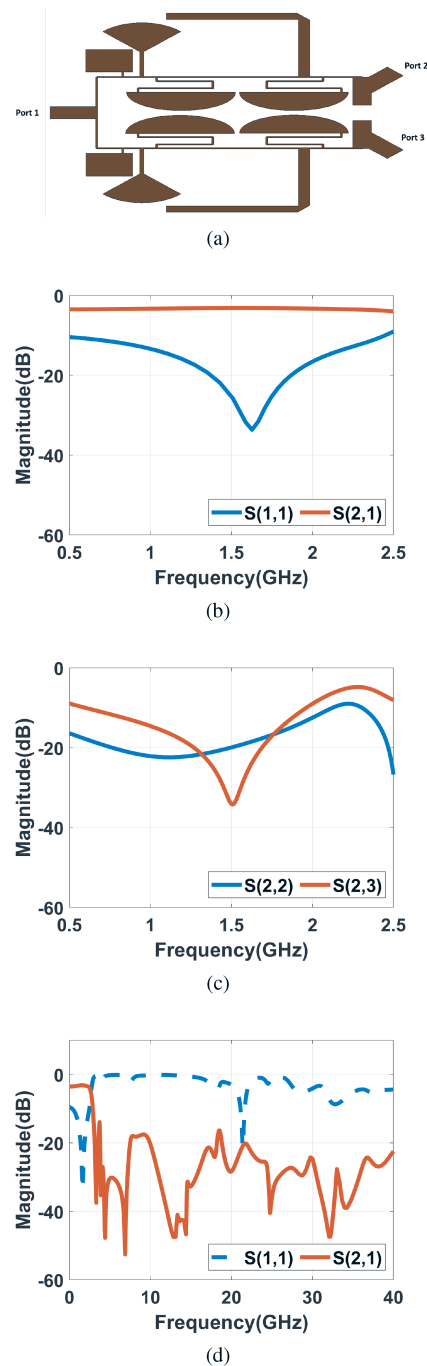
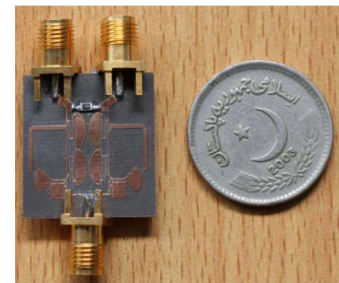
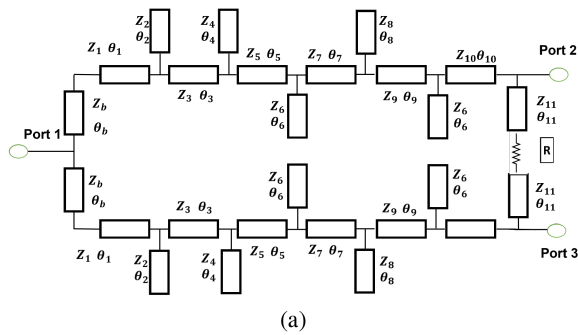


**FIGURE 10.** (a) Layout diagram of proposed power divider (simulated) (b) Frequency response (return loss and insertion loss) in the operating band (0.5 GHz to 2.5 GHz) (c) Frequency response (output return loss and isolations) in the operating band (0.5 GHz to 2.5 GHz) (d) Frequency response of proposed power divider.

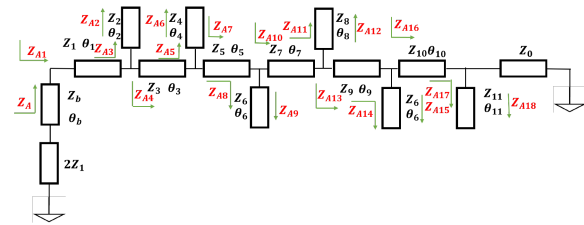
In (1),  $Z_A$  represents the input impedance and is calculated using the even mode equivalent circuit shown in Fig. 11(b). The  $Z_0$  is the characteristic impedance, which is 50 ohms. The remaining impedances  $Z_{A1}$  to  $Z_{A18}$  are calculated in even mode using left-hand side excitation and Fig. 11(b).

Similarly, for calculating the output reflection coefficient, Fig. 11(c) is used where excitation from the right-hand side is

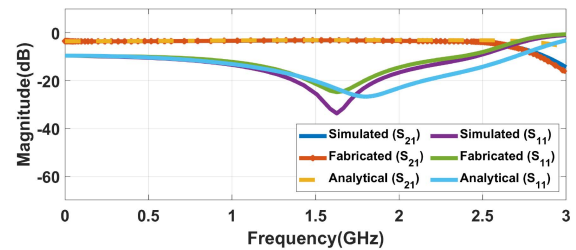


(a)

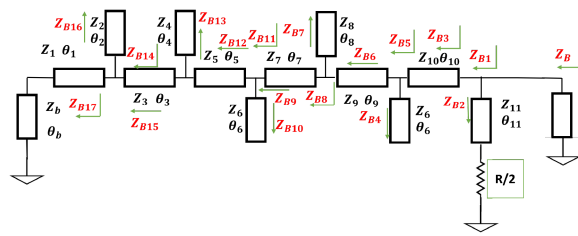
(a)



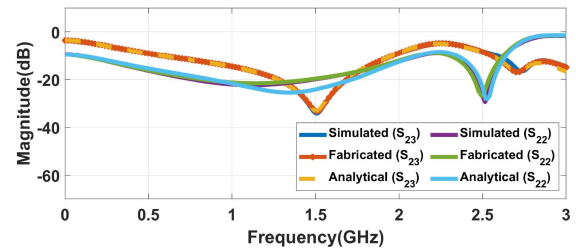
(b)



(b)



(c)



(c)

**FIGURE 11.** (a) An equivalent schematic of the proposed design (b) Even mode equivalent (c) Odd mode equivalent.

**TABLE 1.** Power Divider's Calculated Parameters at 1.64 GHz

Parameters	Calculated value	Parameters	Calculated value
$(Z_b, \theta_b)$	(174.00, 8.8)	$(Z_6, \theta_6)$	(60.03, 17.3)
$(Z_1, \theta_1)$	(174.30, 3.75)	$(Z_7, \theta_7)$	(174.30, 22.3)
$(Z_2, \theta_2)$	(148.30, 7.58)	$(Z_8, \theta_8)$	(103.66, 34.8)
$(Z_3, \theta_3)$	(174.30, 2.68)	$(Z_9, \theta_9)$	(174.30, 2.68)
$(Z_4, \theta_4)$	(149.00, 6.77)	$(Z_{10}, \theta_{10})$	(174.30, 2.68)
$(Z_5, \theta_5)$	(174.30, 2.14)	$(Z_{11}, \theta_{11})$	(82.37, 7.70)

assumed. Output reflection coefficient is calculated using (3).

$$\Gamma_{out}^e = \frac{Z_B - Z_0}{Z_B + Z_0} \quad (3)$$

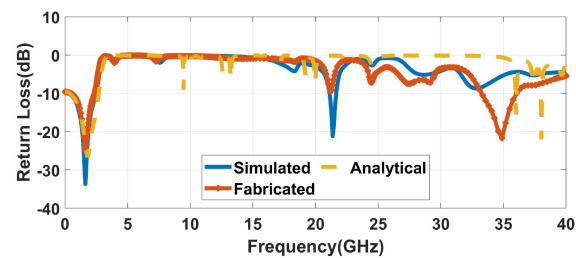
where  $Z_B$  is the output impedance

$$Z_B = \frac{Z_{B1} \cdot Z_{B2}}{Z_{B1} + Z_{B2}} \quad (4)$$

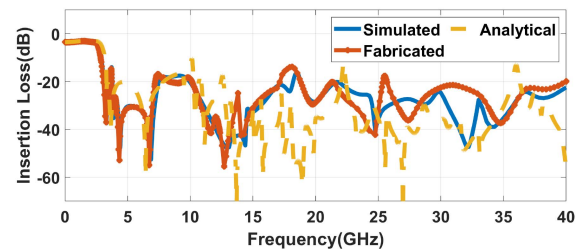
The remaining impedances required for the output impedance,  $Z_{B1}$  to  $Z_{B17}$ , are evaluated using odd mode analysis with right-hand excitation.

The input and output reflection coefficients are used to calculate  $S_{21}$  and  $S_{31}$ .

$$S_{21} = S_{31} = \frac{\Gamma_{in}^e - \Gamma_{out}^e}{2} \quad (5)$$



(d)



(e)

**FIGURE 12.** (a) Snapshot of the proposed fabricated power divider. (b) Measured, simulated, and calculated values of return losses and insertion losses (0-3 GHz). (c) Measured, simulated, and calculated values of output return losses and isolations (0-3 GHz). (d) Measured, simulated, and calculated values of return loss (0-40 GHz). (e) Measured, simulated, and calculated values of insertion loss (0-40 GHz).

**TABLE 2.** Comparison of the Proposed Power Divider's Performance and of Related State-of-the-Art Dividers

Refs.	$f_0$ (GHz)	FBW (%)	RL (dB)	IL (dB)	Harmonics Suppression	Isolation	Size ( $\lambda_g \times \lambda_g$ )
[6]	1	43	20	3.20	2nd to 5th	20	$0.43 \times 0.34$
[7]	2.45	62.07	20	3.40	2nd to 7th	11	$0.19 \times 0.25$
[8]	3.16	104.5	15	3.66	2nd to 5th	15	$0.12 \times 0.15$
[9]	1	39.2	15	3.60	2nd to 4th	32	$0.20 \times 0.16$
[10]	1.09	41.9	16.2	3.80	2nd to 12th	21	$0.26 \times 0.14$
[11]	2.87	23	15	4.10	2nd to 8th	20	$0.46 \times 0.23$
[14]	1.28	12.5	20	4.20	2nd to 6th	36	$0.05 \times 0.15$
[15]	2.4	N/A	38	3.30	2nd to 8th	40	$0.09 \times 0.09$
[16]	1.8	25.8	N/A	3.50	2nd to 11th	17	$0.25 \times 0.15$
[17]	2.2	49	21	3.55	2nd to 5th	20	$0.51 \times 0.14$
[18]	1.27	7	15	4.77	2nd to 3rd	20	N/A
[21]	0.77	38	20	3.99	2nd to 5th	20	$0.04 \times 0.18$
<b>This work</b>	<b>1.64</b>	<b>57</b>	<b>36</b>	<b>3.03</b>	<b>2nd to 24th</b>	<b>23</b>	<b><math>0.15 \times 0.15</math></b>

The associated insertion loss is calculated using (5) [24].

$$IL(\text{dB}) = -20 \cdot \log |S_{21}| \quad (6)$$

In Table 1, all impedances are given, which helps to calculate the design return loss and insertion loss and to plot the calculated results. The resistance, denoted as R, is precisely 100 ohms. The equations for return loss and insertion loss are given in (2) and (6) respectively.

### III. RESULTS AND DISCUSSION

The power divider investigated in this study was implemented on a Rogers 5880 substrate, known for its relative permittivity of 2.2. The substrate's characteristics include a loss tangent of 0.004 and a thickness of 0.787 mm. Simulations were conducted using Advanced Design System (ADS) software, and the resulting design and its outcomes are depicted in Fig. 12(a)–(e).

Fig. 12(a) provides a visual representation of the fabricated design, while Fig. 12(b) presents the simulated, measured, and calculated return loss and insertion loss within the designated operating band. Fig. 12(c) presents the simulated, measured, and calculated output return loss and isolation within the designated operating band. The power divider was measured using an Anritsu MS46122B network analyzer, covering a frequency range from 1 MHz to 43.5 GHz. High-frequency 2.92 connectors (model no K8400A-0000) capable of operating up to 40 GHz were employed, and calibration was performed using the Anritsu MS46122B calibration kit through the short-open-load-through (SOLT) method.

Fig. 12(d) demonstrates good agreement between the simulated, analytical, and measured return loss characteristics. Analytical design results were obtained by calculating an equivalent diagram based on Fig. 7(a), incorporating the values from Table 1. The power divider is designed to operate at 1.64 GHz, with an operating band spanning from 1.151 GHz to 2.083 GHz. The bandwidth of the operating band is 900 MHz, corresponding to a fractional bandwidth (FBW) of 57%.

Fig. 12(e) showcases the insertion loss as simulated, analytical, and measured. With a fractional rejection bandwidth of 170%, the insertion loss remains below  $-15$  dB within the stopband from 3.24 GHz to 40 GHz. The power divider effectively suppresses a total of 24 harmonics, with suppression levels greater than  $-35$  dB for the second, third, eighth, fifteenth, and twenty-first harmonics.

The proposed power divider possesses overall dimensions of  $0.15 \lambda_g \times 0.15 \lambda_g$ , where  $\lambda_g$  represents the free space wavelength at the operating frequency. To evaluate the performance of the proposed design, experimental measurements were conducted and compared to previous literature. The comprehensive comparison, as presented in Table 2, encompasses various performance parameters such as fractional bandwidth (FBW), return loss (RL), harmonic suppression, isolation, and size. The proposed design demonstrates a wide fractional bandwidth of 57% and an ultra-wide suppression bandwidth, outperforming existing designs by achieving the largest FBW and suppressing the 2nd to 24th harmonics. Moreover, it exhibits the lowest return loss of  $-36$  dB among the presented designs. In terms of isolation and physical size, the proposed design also exhibits favorable characteristics compared to state-of-the-art designs.

Regarding in-band performance, the power divider achieves an insertion loss of  $-3.03$  dB and an output return loss of  $-18$  dB. In conclusion, the presented power divider showcases a wide operating band, high selectivity, significant in-band isolation, a simple design, and remarkable ultra-wide harmonic suppression. These attributes make it highly promising for practical applications.

### IV. CONCLUSION

This study describes a power divider with a wide operating range and ultra-wide harmonics reduction capability. Ultra-wide band harmonic suppression is achieved by integrating a novel structure with the transmission lines of a standard Wilkinson power divider. Simulation and measurement results show that harmonics up to 40 GHz are suppressed. The detailed comparison of performance demonstrates that the proposed design outperforms the current state of the art.



REFERENCES

[1] D. M. Pozar, *Microwave Engineering*. Hoboken, NJ, USA: Wiley, 2011.

[2] E. J. Wilkinson, "An N-way hybrid power divider," *IRE Trans. Microw. Theory Techn.*, vol. 8, no. 1, pp. 116–118, Jan. 1960.

[3] S. Roshani, S. Roshani, and A. Zarinitabar, "A modified wilkinson power divider with ultra harmonic suppression using open stubs and lowpass filters," *Analog Integr. Circuits Signal Process.*, vol. 98, no. 2, pp. 395–399, 2019.

[4] G. Zhang, X. Wang, J.-S. Hong, and J. Yang, "A high-performance dual-mode filtering power divider with simple layout," *IEEE Microw. Wireless Compon. Lett.*, vol. 28, no. 2, pp. 120–122, Feb. 2018.

[5] K.-K. M. Cheng and W.-C. Ip, "A novel power divider design with enhanced spurious suppression and simple structure," *IEEE Trans. Microw. Theory Techn.*, vol. 58, no. 12, pp. 3903–3908, Dec. 2010.

[6] Y. Wu, Z. Zhuang, Y. Liu, L. Deng, and Z. Ghassemlooy, "Wideband filtering power divider with ultra-wideband harmonic suppression and isolation," *IEEE Access*, vol. 4, pp. 6876–6882, 2016.

[7] Y. Wang, X.-Y. Zhang, F.-X. Liu, and J.-C. Lee, "A compact bandpass wilkinson power divider with ultra-wide band harmonic suppression," *IEEE Microw. Wireless Compon. Lett.*, vol. 27, no. 10, pp. 888–890, Oct. 2017.

[8] C.-W. Tang and J.-T. Chen, "A design of 3-dB wideband microstrip power divider with an ultra-wide isolated frequency band," *IEEE Trans. Microw. Theory Techn.*, vol. 64, no. 6, pp. 1806–1811, Jun. 2016.

[9] Z. Wang, Z. Zhu, Y. Fu, P. Han, H. Liu, and S. Fang, "A miniaturized balanced-to-unbalanced in-phase filtering power divider with wide upper stopband and wideband common-mode suppression," *IEEE Access*, vol. 9, pp. 143181–143187, 2021.

[10] C. Zhu, J. Xu, W. Kang, and W. Wu, "Microstrip multifunctional reconfigurable wideband filtering power divider with tunable center frequency, bandwidth, and power division," *IEEE Trans. Microw. Theory Techn.*, vol. 66, no. 6, pp. 2800–2813, Jun. 2018.

[11] C. Han, D. Tang, Z. Deng, H. J. Qian, and X. Luo, "Filtering power divider with ultrawide stopband and wideband low radiation loss using substrate integrated defected ground structure," *IEEE Microw. Wireless Compon. Lett.*, vol. 31, no. 2, pp. 113–116, Feb. 2021.

[12] L. Yang, M. Fan, F. Chen, J. She, and Z. Feng, "A novel compact electromagnetic-bandgap (EBG) structure and its applications for microwave circuits," *IEEE Trans. Microw. Theory Techn.*, vol. 53, no. 1, pp. 183–190, Jan. 2005.

[13] M. Li, Y. Wu, M. Qu, Q. Li, and Y. Liu, "A novel power divider with ultra-wideband harmonics suppression based on double-sided parallel spoof surface plasmon polaritons transmission line," *Int. J. RF Microw. Comput.-Aided Eng.*, vol. 28, no. 4, 2018, Art. no. e21231.

[14] G. Shen, W. Che, W. Feng, and Q. Xue, "High-isolation topology for filtering power dividers based on complex isolation impedance and surface wave suppression," *IEEE Trans. Microw. Theory Techn.*, vol. 69, no. 1, pp. 43–53, Jan. 2021.

[15] M. B. Jamshidi, S. Roshani, J. Talla, S. Roshani, and Z. Peroutka, "Size reduction and performance improvement of a microstrip wilkinson power divider using a hybrid design technique," *Sci. Rep.*, vol. 11, no. 1, pp. 1–15, 2021.

[16] S. Roshani, S. Koziel, S. Roshani, M. B. Jamshidi, F. Parandin, and S. Szczepanski, "Design of a patch power divider with simple structure and ultra-broadband harmonics suppression," *IEEE Access*, vol. 9, pp. 165734–165744, 2021.

[17] W. Feng, X. Ma, R. Gómez-García, Y. Shi, W. Che, and Q. Xue, "Multi-functional balanced-to-unbalanced filtering power dividers with extended upper stopband," *IEEE Trans. Circuits Syst. II: Exp. Briefs*, vol. 66, no. 7, pp. 1154–1158, Jul. 2019.

[18] Y. Zhu, J. Wang, J. Hong, J.-X. Chen, and W. Wu, "Two-and three-way filtering power dividers with harmonic suppression using triangle patch resonator," *IEEE Trans. Circuits Syst. I, Reg. Papers*, vol. 68, no. 12, pp. 5007–5017, Dec. 2021.

[19] R. Pouryavar, F. Shama, and M. A. Imani, "A miniaturized microstrip wilkinson power divider with harmonics suppression using radial/rectangular-shaped resonators," *Electromagnetics*, vol. 38, no. 2, pp. 113–122, 2018.

[20] M. A. Imani, F. Shama, M. Alirezapoori, S. Haghiri, and A. Ghadrdan, "Ultra-miniaturized wilkinson power divider with harmonics suppression for wireless applications," *J. Electromagn. Waves Appl.*, vol. 33, no. 14, pp. 1920–1932, 2019.

[21] G. Shen, W. Che, Q. Xue, and W. Feng, "Novel design of miniaturized filtering power dividers using dual-composite right-/left-handed resonators," *IEEE Trans. Microw. Theory Techn.*, vol. 66, no. 12, pp. 5260–5271, Dec. 2018.

[22] M. S. Gilan and F. Gholami, "Design and fabrication of an ultra compact gysel power divider with harmonic suppression by using u shaped resonators," *Frequenz*, vol. 77, no. 1–2, pp. 23–27, 2023.

[23] W. Zhao, Y. Wu, Y. Yang, and W. Wang, "Novel on-chip wideband filtering power dividers with high selectivity and ultra-wide out-of-band suppression in LTCC technology," *IEEE Trans. Circuits Syst. II, Exp. Briefs*, vol. 69, no. 11, pp. 4288–4292, Nov. 2022.

[24] M.-T. Chen and C.-W. Tang, "Design of the filtering power divider with a wide passband and stopband," *IEEE Microw. Wireless Compon. Lett.*, vol. 28, no. 7, pp. 570–572, Jul. 2018.



**SIKANDAR ABBAS** (Student Member, IEEE) received the B.S. degree in electrical engineering from the University of Lahore, Lahore, Pakistan, in 2018, and the M.S. degree in electrical engineering from the Institute of Space Technology (IST), Islamabad, Pakistan, in 2022. He is currently a Research Assistance with Nanotech Lab, Information Technology University, Lahore. His current research interests include antennas, power dividers and microwave components



**MOAZAM MAQSOOD** (Member, IEEE) was born in Faisalabad, Pakistan, in 1983. He received the B.Sc. degree in communication systems engineering from the Institute of Space Technology, Islamabad, Pakistan, in 2006, and the M.S. degree in microwave engineering and wireless subsystem design and the Ph.D. degree in integrated antennas and arrays for GNSS from the University of Surrey, Guildford, U.K, in 2009 and 2013, respectively. He is currently an Assistant Professor with the Department of Electrical Engineering, Institute of Space Technology.



**NOSHERWAN SHOAB** (Senior Member, IEEE) received the master's degree in electronics engineering and the Ph.D. degree in radio-frequency and microwave engineering from Politecnico di Torino, Turin, Italy. After serving two terms as a Postdoctoral Research Fellow, he joined the National University of Sciences and Technology, Islamabad, Pakistan. As an Associate Professor, he is mainly engaged in 5G antenna design, the development of metasurfaces, energy harvesting, and the Internet of Things.



**MUHAMMAD QASIM MEHMOOD** (Senior Member, IEEE) received the Ph.D. degree in electrical and computer engineering from the National University of Singapore, Singapore, in 2016. He is currently an Associate Professor with the Electrical Engineering Department, Information Technology University, Lahore, Pakistan. His research interests include RF and microwave engineering, optics, and nanophotonics, more precisely the demonstration of exotic phenomena via ultrathin nanostructured devices, e.g., on-chip orbital angular manipulation,

beam steering, spin-orbital coupling, holography, polarization filtering, and light absorption.



**MUHAMMAD ZUBAIR** (Senior Member, IEEE) received the Ph.D. degree in electronic engineering and telecommunications from the Politecnico di Torino, Turin, Italy, in 2015. From 2015 to 2017, he was a Postdoctoral Research Fellow with the Singapore University of Technology and Design/Massachusetts Institute of Technology SUTD-MIT International Design Centre International Design Centre, Singapore. In November 2017, he joined the Information Technology University, Lahore, Pakistan, as an Assistant Professor

where he was promoted to Associate Professor in May 2021. He was a Visiting Faculty with the SUTD and King Abdullah University of Science and Technology (KAUST), Thuwal, Saudi Arabia. He is currently with the Innovative Technologies Laboratories (ITL) at KAUST. His recent research interests include fractional methods in modeling and simulation of complex systems including smart city applications, applied and computational photonics, microwave imaging hardware for biomedical applications, design of electromagnetic metamaterials, reconfigurable metasurfaces for 6G applications, and AI based electromagnetic design. He was the recipient of the Punjab Innovation Research Challenge Award 2021 for this project, Young Scientist Award by the International Union of Radio Science (URSI) in the URSI General Assembly (GASS 2021, Rome). He serves on the editorial board of *PLOS One* and *International Journal of Antennas and Propagation* and was an Associate Editor for the IEEE ACCESS, and the *IET Microwaves, Antennas and Propagation*.



**YEHIA MASSOUD** (Fellow, IEEE) received the Ph.D. degree in electrical engineering and computer science from the Massachusetts Institute of Technology, Cambridge, MA, USA. He has held several experiences at leading institutions of higher education and respected industry names, including Rice University, Houston, TX, USA, Stevens Institute of Technology, Hoboken, NJ, USA, Worcester Polytechnic Institute, Worcester, MA, USA, UAB, the SLAC National Accelerator Laboratory, and Synopsys Inc. From 2018 to 2021, he was the Dean

of the School of Systems and Enterprises (SSE), Stevens Institute of Technology. Prior to Stevens, he was the Head of the Department of Electrical and Computer Engineering, Worcester Polytechnic Institute, from 2012 to 2017. In 2003, he joined Rice University, as an Assistant Professor, where he became one of the fastest Rice Faculty to be granted tenure with the Department of Electrical Engineering and the Department of Computer Science, in 2007. He is currently a Professor and the Director of the Innovative Technologies Laboratories (ITL), King Abdullah University of Science and Technology, Thuwal, Saudi Arabia. He has authored or coauthored more than 550 papers in leading peer-reviewed journals and conference publications. His research interest includes design of state-of-the-art innovative technological solutions that span over the broad range of technical areas, including smart cities, autonomy, smart health, embedded systems, nanophotonics, and spintronics. He was the recipient of the Rising Star of Texas Medal, the National Science Foundation CAREER Award, the DAC Fellowship, the Synopsys Special Recognition Engineering Award, and several best paper awards. He was selected as one of ten MIT Alumni Featured by the MIT's Electrical Engineering and Computer Science Department, in 2012. He was named a Distinguished Lecturer by the IEEE Circuits and Systems Society, from 2014 to 2015. He was the Editor of the *Mixed-Signal Letters-the Americas*, as an Associate Editor for IEEE TRANSACTIONS ON VERY LARGE SCALE INTEGRATION (VLSI) SYSTEMS, and IEEE TRANSACTIONS ON CIRCUITS AND SYSTEMS—I: REGULAR PAPERS, as well as the Guest Editor for a Special Issue of IEEE TRANSACTIONS ON CIRCUITS AND SYSTEMS—I: REGULAR PAPERS.